Tribology International 43 (2010) 667–675

Contents lists available at ScienceDirect

Tribology International

journal homepage: www.elsevier.com/locate/triboint

Tribological behaviors of surface-coated serpentine ultrafine powders as lubricant additive

H.L. Yu [a,*], Y. Xu [a], P.J. Shi [a], H.M. Wang [a], Y. Zhao [a], B.S. Xu [a], Z.M. Bai [b]

[a] National Key Laboratory for Remanufacturing, Academy of Armored Forces Engineering, 100072 Beijing, PR China
[b] School of Material Science and Engineering, China University of Geosciences, 100083 Beijing, PR China

ARTICLE INFO

Article history:
Received 11 December 2008
Received in revised form
1 August 2009
Accepted 12 October 2009
Available online 17 October 2009

Keywords:
Serpentine
Ultrafine powder
Additive
Tribological property

ABSTRACT

The effect of surface-coated ultrafine powders (UFPs) of serpentine suspended in lubricants on the tribological behaviors of a mated 1045 steel contact was investigated. Through the addition of serpentine UFPs to oil, the wear resistance ability was improved and the friction coefficient was decreased. The addition of 1.5 wt% serpentine to oil is found most efficient in reducing friction and wear. The nano-hardness and the ratio of hardness to modulus of friction surface are observably increased. Such effects can be attributed to the formation of a tribofilm of multi-apertured oxide layer, on which the micrometric alumina particles embedded and serpentine nano-particles adsorbed.

1. Introduction

Over the last few years, interest in the synthesis and tribological properties of ultrafine powders (UFPs) as lubricant additives has steadily grown due to their efficacies in reducing friction and wear [1–4]. There have been many investigations on the behaviors of inorganic or organic UFPs as extreme pressure (EP) and anti-wear (AW) additives for liquid lubricants. It is found that the lubricating properties of oils were significantly improved when nano-sized particles were used, while micro-sized particles had much smaller effects [5–7].

Compared with nano-particles, the micrometric UFPs in liquid media are more thermodynamically unstable and tend to spontaneously subside. The large-scale particles, on the other hand, can act as abrasive particles on contacts, as accordingly result in severe wear. Therefore, the previous and current studies on UFPs additives mainly focused on the tribology testing of nano-scale particles of metals [8–13], carbon materials [14–17], oxides [18–20], sulfides [21–23], borates [24], RE compounds [25–27], polymers [28], etc. Besides BN particles [29,30], few studies were carried out on micro-sized UFPs due to their small contribution towards friction-reducing and wear resistance.

Serpentine group describes a group of common rock-forming hydrous magnesium iron phyllosilicate ($(Mg,Fe)_6Si_4O_{10}(OH)_8$) minerals. They may contain minor amounts of other elements including chromium, manganese, cobalt and nickel. Recent researches indicate the micro-sized serpentine ($Mg_6[Si_4O_{10}](OH)_8$) UFPs present excellent tribological properties when added to liquid lubricants [31,32]. Jin et al. [33] investigated the tribological behaviors of crankcase oil suspended serpentine particles ($\leq 2.0\,\mu m$) in railway diesel engines under field trial conditions. They found that a super-hard and super-lubricious oxide layer formed on the worn ferrous surface, as accordingly lowers the friction and wear. Yu et al. [34] studied the lubricating effect of natural mineral admixtures (size: 0.3–3 μm) that mainly composed of serpentine (90–95%) and schungite (4.8–9.8%). They found that a DLC film with Si or Si–O structures doped formed on the worn steel contacts, as contributes to the excellent mechanical and tribological properties of the friction surface.

The present study aimed to further clarify the mechanisms responsible for the effect of serpentine minerals used as additives. The effect of surface-coated serpentine UFPs, with an average particle size of 1.0 μm, suspended in lubricating oils on the tribological behaviors of steel contact was reported. The morphologies and element distributions of the tribofilm formed by the serpentine were studied. In particular, the nano-mechanical properties of the tribofilm were measured by a nano-indentation tester.

2. Experimental

2.1. Materials

The UFPs used in the present study were prepared by mechanical crushing and ball-milling the serpentine mineral

* Corresponding author. Tel.: +86 10 66718580; fax: +86 10 66717144.
E-mail address: helong.yu@163.com (H.L. Yu).

0301-679X/$ - see front matter © 2009 Elsevier Ltd. All rights reserved.
doi:10.1016/j.triboint.2009.10.006

Table 1
Chemical composition of the serpentine minerals.

Oxides	Content (wt%)
SiO_2	43.49
Al_2O_3	1.18
FeO	0.25
MnO	0.32
MgO	41.0
CaO	0.64
K_2O	0.33
P_2O_5	0.085
H_2O^+	12.37
H_2O^-	0.29

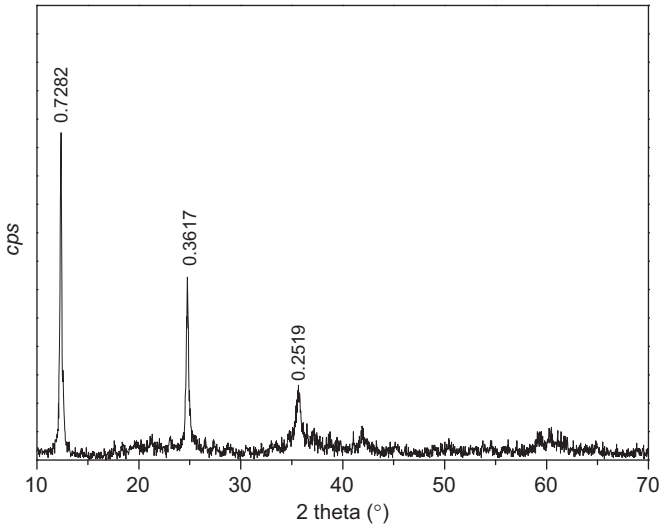

Fig. 1. XRD pattern of untreated serpentine UFPs.

(Liaoning Province, China). Table 1 lists the chemical compositions of the starting materials, its crystal formula can be expressed as $Mg_{5.70}Al_{0.13}Fe_{0.02}Ca_{0.06}K_{0.04}Mn_{0.03}[Si_{4.05}O_{10}](OH)_8$, which is close to the ideal formula of serpentine, i.e. $Mg_6[Si_4O_{10}](OH)_8$. Fig. 1 shows the X-ray diffraction pattern of the ball-milled serpentine UFPs. The diffraction peaks of d=0.7282, 0.3617 and 0.2519 nm can be indexed to those of antigorite, corresponding to the (0 0 1), (1 0 2), and (16.0.1) planes, respectively. Its lattice parameters are calculated as follows: a=0.536 nm, b=0.928 nm, c=0.732 nm, $\alpha=\gamma=90^\circ$ and $\beta=91.38^\circ$, further proving the antigorite structure. To provide good stabilization in viscous liquid, a mixture of boric acid ester and Span 60 (mol. ratio=1:1) was mixed with the UFPs in a globe mill for 6 h operation (rotating speed=300 rpm) to produce an organic coating layer. Fig. 2 shows the SEM image and size distribution of the surface-coated serpentine UFPs. The particle size is mostly in the range of 0.1–5 μm and the average size approximates 1.0 μm. The final surface-coated UFPs can be dispersed well in some organic solvents, such as chloroform, benzene, methylbenzene and lubricating oil.

2.2. Friction and wear test

An MM-10 W sliding friction tribotester was employed to study the friction-reduction and anti-wear abilities. As shown schematically in Fig. 3, the MM-10 W comprises an upper rotating ring specimen, which came into contact with a lower disk specimen fixed in an oil bath. The friction coefficient and temperature of the disk specimen were then measured. Diesel engine oil (grade:

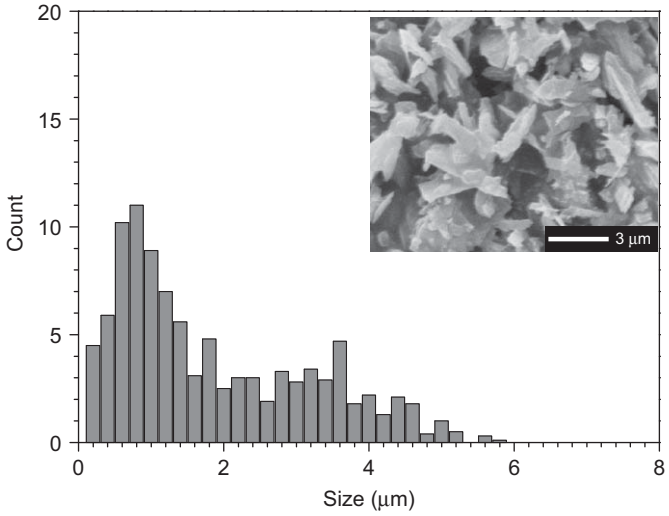

Fig. 2. SEM image and size distribution of surface-coated serpentine UFPs.

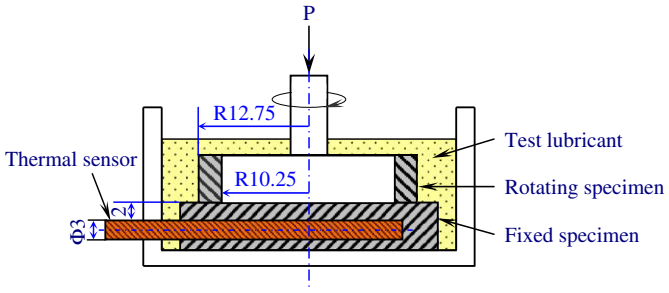

Fig. 3. Schematic illustration of friction and wear test.

Table 2
Viscosity of oil with and without serpentine UFPs.

	Kinematic viscosity (100 °C) (mm^2/s)	Viscosity (150 °C, 10^6 s) (mPa s)
Pure oil	18.6	3.7
0.5 wt% UFPs	18.6	3.7
1.0 wt% UFPs	18.6	3.7
1.5 wt% UFPs	18.7	3.7
2.0 wt% UFPs	18.7	3.8

50 CC) was used as a lubricant for the friction specimens of the rings and disks (1045 steel, hardness: 210 HB, surface roughness: 0.20–0.25 μm). Table 2 gives viscosity of the oil with and without serpentine UFPs. High-energy mechanical ball-milling agitation (rotating speed=120 rpm, duration=60 min) and ultrasonic dispersion (power=200 W, temperature=40 °C, duration=30 min) were used to provide good dispersion stability of the surface-coated UFPs in oil. The experimental conditions were: atmospheric environment, room temperature, normal load=100, 200, 300 and 400 N, sliding speed=1.51 m/s and test duration=120 min. The corresponding initial mean Hertzian pressure at the contacts was 0.554 MPa (100 N), 1.11 MPa (200 N), 1.66 MPa (300 N) and 2.21 MPa (400 N). After the test, the steel disks were cleaned in petroleum ether and absolute ethyl alcohol. The wear rates of the disks were then calculated by

measuring the weight loss of the disks using a mass balance to an accuracy of 0.1 mg. All the experimental results were the average of three sets of the experimental data.

2.3. Worn surface analysis

Scanning electronic microscope (SEM) equipped with energy dispersive X-ray spectroscopy (EDS) was utilized to analyze the morphologies and element distributions of the worn steel disks. Nano-indentation tester (Nano Test 600, Micro Materials Ltd.) was utilized to investigate the mechanical properties of the rubbing surfaces. A three sided pyramidal diamond indenter, with a diameter of 50 nm, was used throughout the test. In a constant maximal load test, the initial and maximum load was 0.03 and 15 mN, respectively. The loading and unloading rates were both 0.3 mN/s, and the dwell time at maximum load was 60 s. In constant maximal indentation depth tests, the maximal depth of indentation was controlled as follows: 50, 100, 200, 500, 1000, 1500 and 2000 nm. The initial load was 0.03 mN. The loading and unloading rates were both 0.3 mN/s. In order to avoid the interaction between two test points, distance between any two points was not shorter than 10 μm.

3. Results

3.1. Tribological properties

Fig. 4 shows the variation of friction coefficient with applied load for oil with and without serpentine UFPs. The coefficient of pure oil increases linearly along with the increasing normal load. With the addition of serpentine to oil, the friction decreases at all applied loads. The best friction-reduction property can be obtained when the UFPs concentration is 1.5 wt%. Such concentration decreases the friction coefficient by 50.6% at 100 N, 58.1% at 200 N, 56.3% at 300 N and 56.1% at 400 N, as compared to pure oils. When the concentration is higher than that, the friction-reduction property is weakened, but still superior to pure oil.

During the friction test, the specimen temperature can be measured by the sensor that inserted in the disk. Fig. 5 demonstrates time dependency of specimen temperature at applied load of 200 N. It shows that the temperature of disks lubricated with oil containing UFPs is lower than that of pure oil. Similar with the results of friction coefficient, the lowest

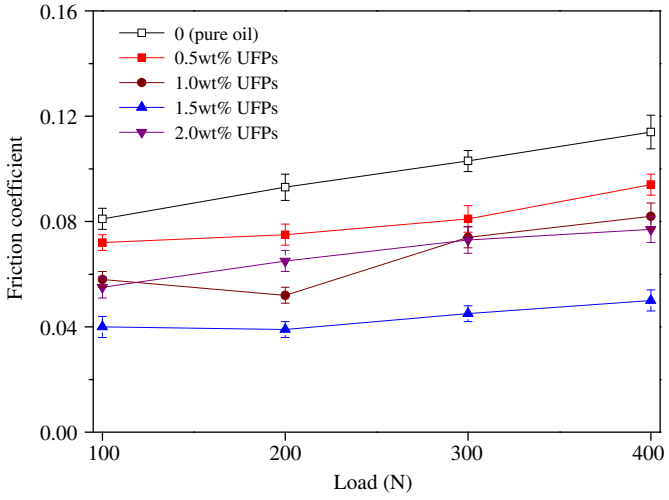

Fig. 4. Variation of friction coefficient with normal load.

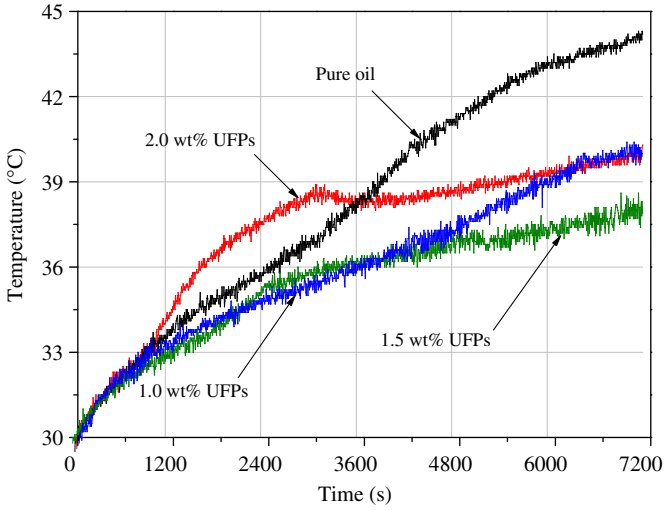

Fig. 5. Friction time dependency of specimen temperature (normal load=200 N).

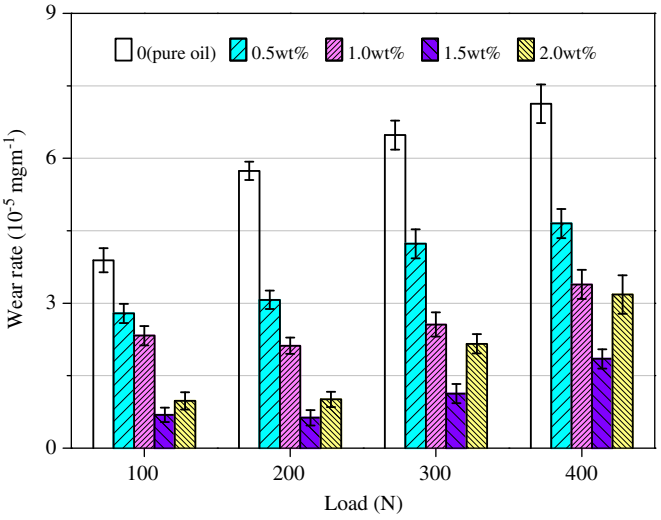

Fig. 6. Wear rate of disk specimens under the lubrication of oil with and without serpentine UFPs.

specimen temperature is obtained when serpentine concentration is 1.5 wt%. The corresponding temperature decreases by 13.5% compared to pure oil. It is known that when surfaces slide relatively, almost all the energy dissipated in friction appears in the form of heat at the interface. This frictional heat raises the temperature of specimen and oil. It is noted that the 2.0 wt% suspension causes a higher temperature with regard to the rest of samples during the first half of friction tests. That may be caused by local breakage of oil film initiated by increasing solid particles of serpentine in the beginning compared with lower concentration, as resulted in higher friction and specimen temperature.

Fig. 6 shows the anti-wear property of oil with and without serpentine UFPs versus applied load. Wear of disk specimens under the lubrication of oil with and without serpentine increases with the increasing load. With the addition of the UFPs to oil, the wear of steel disk is reduced. Similar with the variation of friction coefficient, the best anti-wear property can be obtained when serpentine concentration is 1.5 wt%. As compared to pure oils, such concentration decreases wear rate of disk specimen by 82.3% at 100 N, 89% at 200 N, 82.5% at 300 N and 74.1% at 400 N.

3.2. Morphology and elementary analysis of the worn surface

Typical SEM images of the worn surfaces under the lubrication of oil with and without serpentine (normal load=200 N) are shown in Fig. 7. The obvious furrows and grooves in sliding direction, formed by the wear debris, are wide and deep for the disks lubricated with pure oil, showing severe abrasive wear. The furrows become shallow and narrow when adding 1.0 wt% serpentine to oil. A large number of micro-apertures with a uniform distribution appear on the worn surface. The rubbing surface lubricated with 1.5 wt% suspension is smoother and multi-apertured, few grooves can be found. This result is in accordance with the best tribological behaviors of oil containing 1.5 wt% serpentine.

Fig. 8 shows the magnified morphology and corresponding elemental distribution map of the image shown in Fig. 7(c). Four typical patterns marked as A, B, C and D can be clearly seen on the worn surface lubricated with oil containing 1.5 wt% serpentine UFPs. It is obvious that most areas of the surface are smooth, e.g. zone A. Furthermore, there exist a lot of micro-apertures in which the micro-sized particles (0.5–1 μm), e.g. particle B, and their aggregations (2–3 μm), e.g. particle C, are embedded. At the same time, a large number of nano-sized adsorbates (100–200 nm), e.g. particle D, distribute uniformly on the surface. The elemental distribution maps show the presence of the elements of Fe, O, Al, Si and Mg on the rubbing surface. The relative concentration of Fe is highest, as may be caused by the electronic beam of EDS which penetrated the worn surface and hit directly the substrate steel.

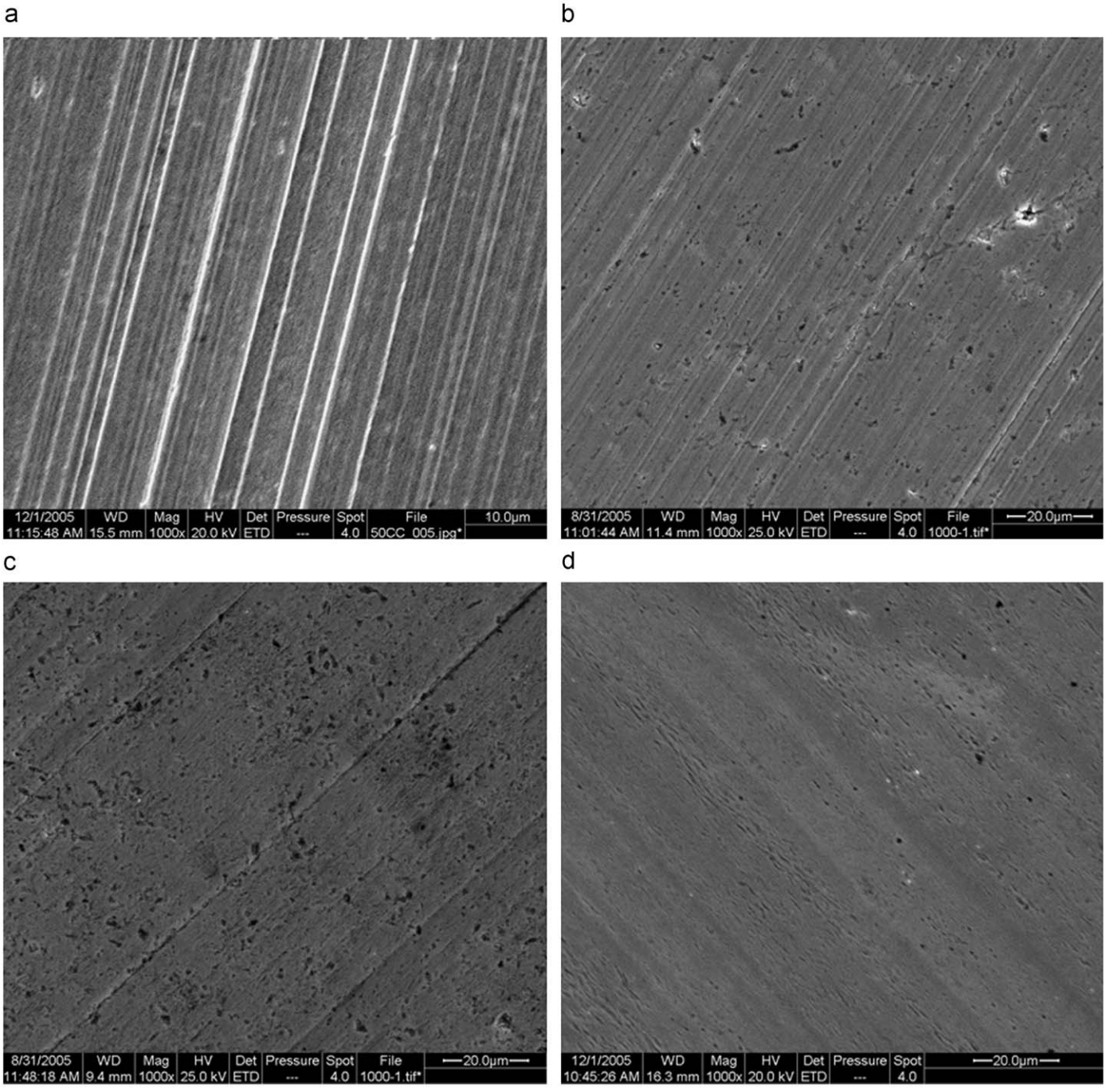

Fig. 7. SEM morphologies of worn surfaces under the lubrication of (a) pure oil, (b) oil+1.0 wt% UFPs, (c) oil+1.5 wt% UFPs and (d) oil+2.0 wt% UFPs (normal load=200 N).

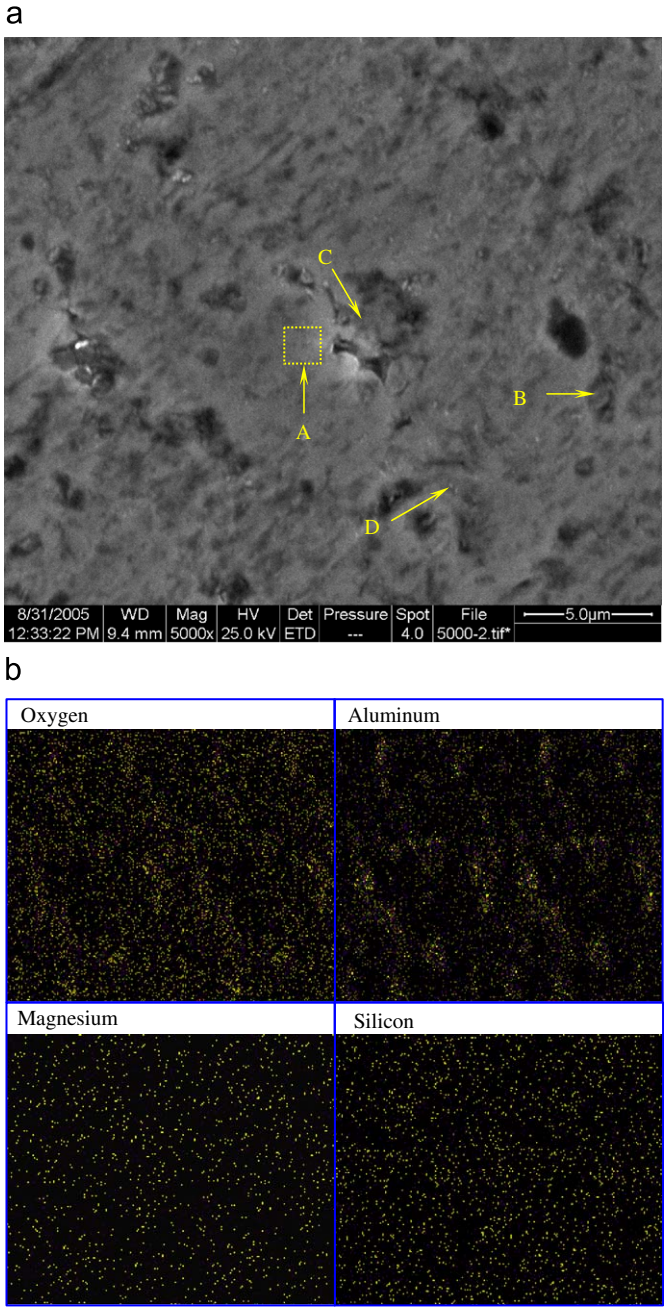

Fig. 8. Enlarged SEM image (a) and elemental distribution (b) of the morphology shown in Fig. 7(c). (Surface lubricate with 1.5 wt% UFPs suspension at a normal load of 200 N.)

Mg and Si distribute uniformly across the surface. While Al exists only in the regions corresponding to the apertures embedded micro-sized particles, where the relative concentration of O is also higher. That indicates the micro-sized particles mainly consist of Al and O.

Fig. 9 shows the EDS patterns of (1) the different worn areas shown in Fig. 8(a) and (2) the surface lubricated with pure oil. Table 3 gives the semiquantitative analysis results. It is obvious that the compositions of regions B and C are similar, mainly containing the elements of O and Al. The ratio of oxygen atom to aluminum atom is about 3 to 2. So, it is inferred that the micro-sized particles embedded in the apertures are alumina (Al_2O_3) particles. Particle D mainly contains O, Si and Mg, showing it is possible the serpentine particles that porphyrized by sliding contacts during friction. It is seen in Fig. 9(c) that the oxygen content of zone A was much higher than that of surface lubricated with pure oil, showing an oxide layer forms. The above-mentioned results indicate that a tribofilm of multi-apertured oxide layer, on which micrometric alumina particles embedded and serpentine nano-particles adsorbed, has formed on worn surface with oil containing serpentine.

3.3. Nano-mechanical properties of the worn surface

It is generally difficult to avoid the effects of substrate when measuring the mechanical properties of thin films. Therefore, mechanical characterization of tribofilms is generally not easy. Many works have been carried out to do that using nano-indentation method [33–38]. Here, two nano-indentation testing methods, namely controlling maximal applied load and maximal indentation depth, were performed to study mechanical properties of normal worn surface (pure oil, normal load = 200 N) and the tribofilm (1.5% UFPs suspension, normal load = 200 N).

Controlling maximum load indentation tests were performed to compare the mechanical properties of different surfaces. Thirty points were chosen at random on the surface of every friction sample to measure their nano-hardness (H) and elastic modulus (E). Fig. 10 shows the typical and total 30 load-depth curves of normal worn surface and the tribofilm tested with a maximal applied load of 15 mN. The maximum indentation depth and plastic deformation for the tribofilm are much smaller than those of normal worn surface, indicating the tribofilm was a hard thin layer. Table 4 lists the nano-hardness and modulus of different worn surfaces. The nano-hardness (H), elastic modulus (E), and their ratio (H/E) of the tribofilm are superior to normal worn surface. The addition of 1.5 wt% serpentine increased the average H of the worn surface by 94%, and increased the mean value of H/E by 75%.

In order to clarify the influence of substrate on the mechanical properties of the tribofilm, indentation tests were performed with different maximal indentation depths. For a given maximal indentation depth, five points were chosen at random on the tribofilm (worn surface lubricated with 1.5 wt% UFPs suspension at load of 200 N). Fig. 11 shows the dependency of H and E on maximal indentation depth. When tested with a maximal depth of 50, 100 and 200 nm, H of the tribofilm approximates 8.2 GPa. The value decreases rapidly with the increasing maximal indentation depth when it is deeper than 200 nm, showing the effects of substrate increase. When the depth reaches 2000 nm, H approximates 3.6 GPa which is in accord with the 1045 steel. The results indicate the real nano-hardness of the tribofilm is approximately 8.2 GPa and its thickness is possible between 200 and 2000 nm.

The ratio of hardness and elastic modulus, H/E, is usually introduced as a main parameter to estimate the relative wear resistance of materials. Fig. 12 demonstrates H/E tested with different maximal indentation depth on normal worn surface and the tribofilm (1.5 wt% UFPs suspension at load of 200 N). The value is about $(1.5 \pm 0.1) \times 10^{-2}$ for normal worn surface with different maximal indentation depths, while it decreases from 3.41×10^{-2} to 1.79×10^{-2} for tribofilm with the increasing maximal indentation depth. The result further indicates the wear resistance property of the tribofilm is superior to the normal worn surface.

4. Discussion

According to the present experimental results, it can be concluded that an oxide tribofilm has formed on the worn surface

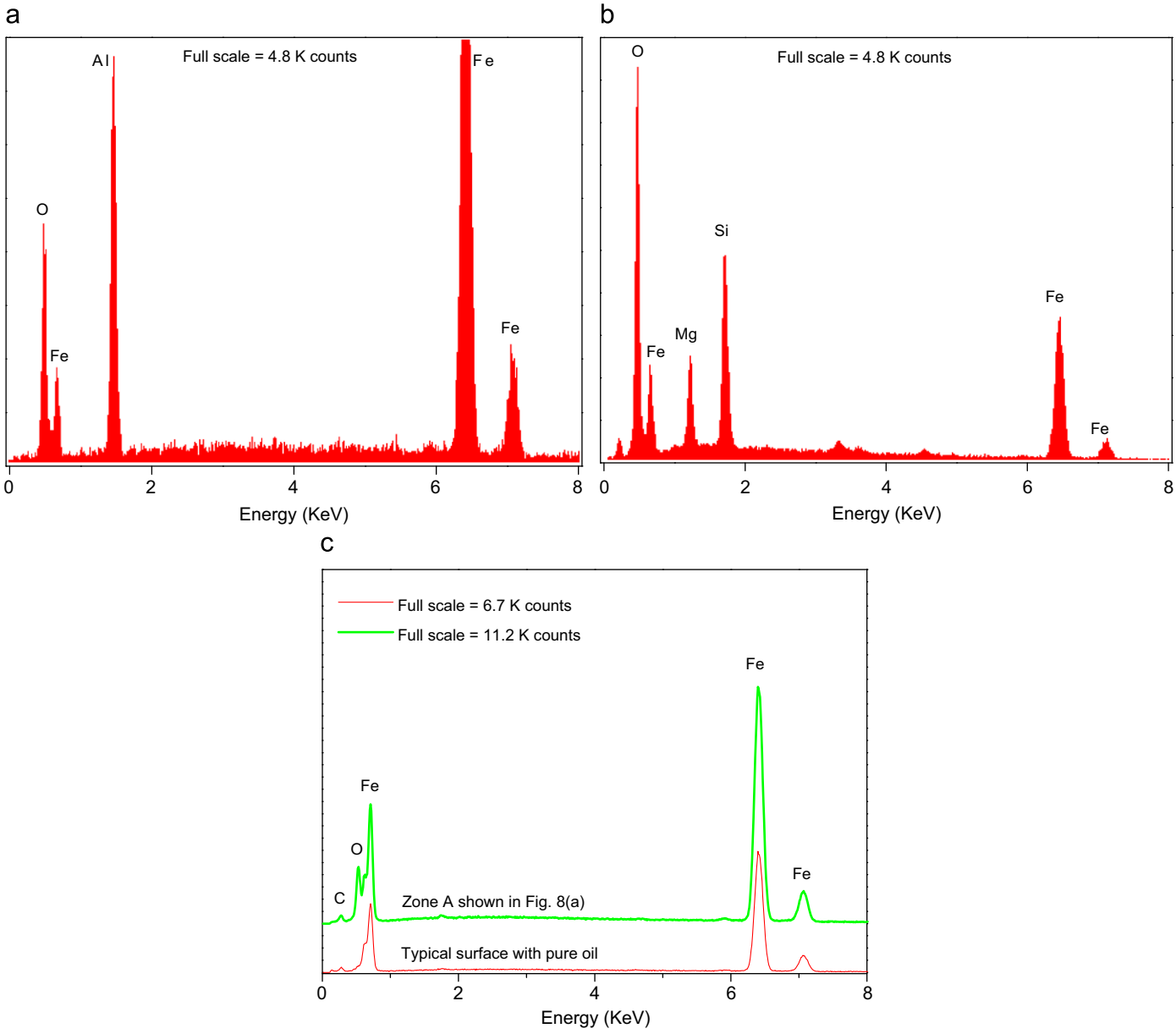

Fig. 9. EDS analysis of (a) particle B, (b) particle D and (c) zone A and surface lubricated with pure oil.

Table 3
Elemental compositions of the different worn zones shown in Fig. 8(a).

	Element composition (at%)					
	Fe	O	Si	Mg	Al	Others
A	84.51	9.68	0.26	0.38	0.25	0.42
B	37.34	33.52	0.60	0.82	27.52	0.20
C	41.92	33.96	0.15	0.20	23.40	0.37
D	77.96	12.40	3.60	5.42	0.17	0.45

under the lubrication of oil with surface-coated serpentine UFPs. The result is similar with what has been reported by Jin et al. [33]. But, what is different from the previous studies is that the tribofilm is a multi-apertured oxide layer on which micrometric alumina particles embedded, and serpentine nano-particles adsorbed. It is obvious that the film consists of three typical structures: (1) oxide layer with excellent nano-mechanical properties, (2) micro-apertures with alumina particles embedded, and (3) third bodies formed by nano-scale serpentine particles.

Serpentine as a typical phyllosilicate has a basic structure of $[SiO_4]$ which is connected by three bridging oxygen atoms between each other, as accordingly forms Si–O tetrahedron layers in two-dimensional space. The non-bridging oxygen atoms in $[SiO_4]$ point to the same direction and connect with Mg^{2+}, and

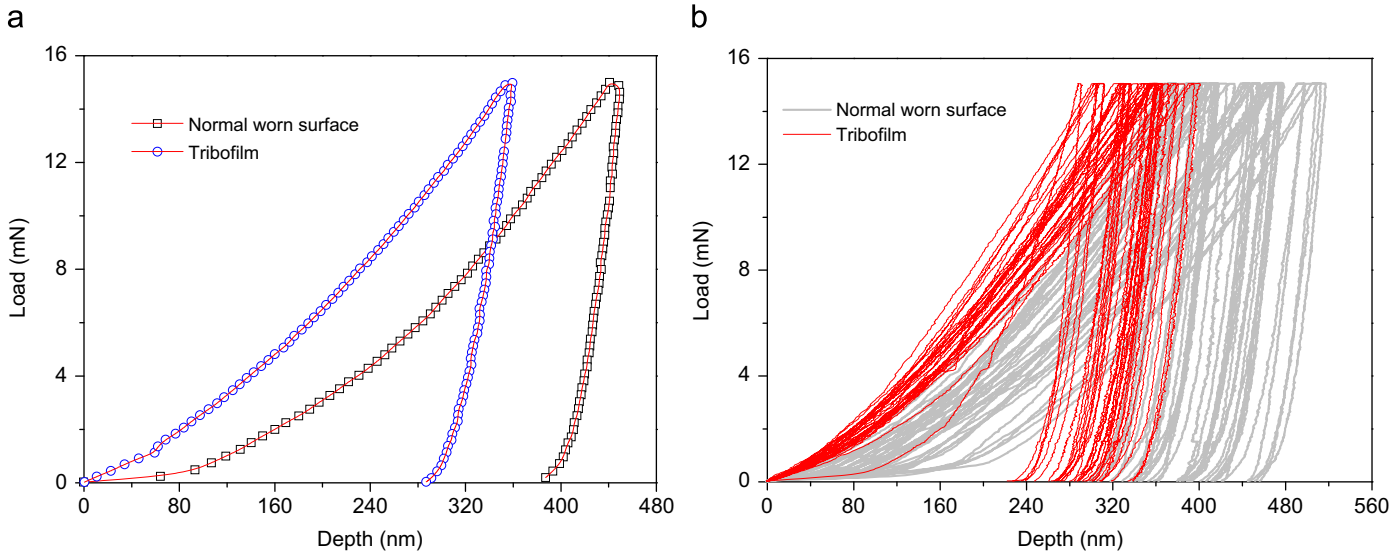

Fig. 10. Typical (a) and total (b) load–depth curves of different surfaces tested by nano-indentation tester with a maximal applied load of 15 mN.

Table 4
Nano-mechanical properties of normal worn surface and the tribofilm measured by controlling the maximal load at 15 mN.

	Nano-mechanical properties				
	Max depth (nm)	Plastic depth (nm)	H (GPa)	E (GPa)	H/E ($\times 10^{-2}$)
Normal surface	438.80 ± 59.70	393.50 ± 54.47	3.45 ± 0.85	215.53 ± 32.10	1.60
Tribofilm	342.55 ± 42.41	289.65 ± 37.57	6.68 ± 0.65	238.52 ± 29.65	2.80

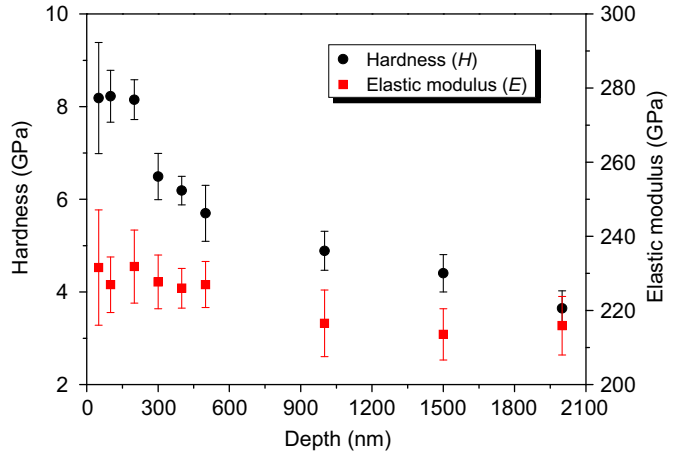

Fig. 11. Dependency of hardness (H) and elastic modulus (E) on maximal indentation depth measured on the tribofilm (1.5 UFPs suspension, 200 N).

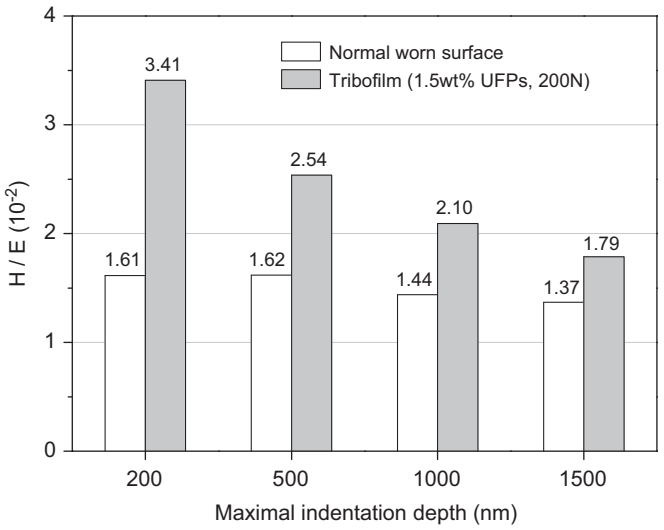

Fig. 12. Dependency of ratio of hardness to elastic modulus on maximal indentation depth.

consequently form Mg–O octahedral layers. The two layers are connected by weak molecular bond and/or hydrogen bond to form the typical layer structure of serpentine, which displays good capability of oxygen release due to the weak bond between the Si–O tetrahedral layer and Mg–O octahedral layer. Mechanical action caused by the direct contact of friction surfaces initiate the crystal fracture of the layered structure of serpentine particles that suspended in oil. Then oxygen atoms and oxygen-containing species were released for the bond breakage of Si–O tetrahedron and Mg–O octahedral. Finally, the mechanochemical/thermochemical oxidation reaction of iron atoms and oxygen atoms occurred [33], and a hard oxide layer was accordingly formed on the worn ferrous surface.

In general, a hard oxide layer can provide a sufficient resistance not only to the embedding of abrasive particles but the plastic deformation of materials in sliding friction as well, the abrasive wear can be accordingly reduced. But, there is no inevitable dependence between the increasing of hardness and the reduction of abrasive wear. Practically, the reduction of elastic modulus usually results in the reducing of wear. That means, for a metal

surface with lower elastic modulus, elastic deformation would more easily occur when contact stress applied, as increases the contact area between the sliding surfaces, and reduces the contact stress. In this case, it is more easily for the abrasive particles to pass the contacts, and consequently reduce the abrasive wear. Physically, the higher is the H/E value, the better is the wear resistance. Nano-indentation test results demonstrate that the formation of an oxide layer increased significantly the average nano-hardness and H/E value of the rubbing surface under lubrication of oil with serpentine. That may be the main reason why the wear resistance property of worn surface was improved.

The UFPs used in the present study were prepared from natural minerals of serpentine which was impure and contained a small amount of Al atoms. That means Al^{3+} substituted for Mg^{2+}, connected with the non-bridging oxygen atoms in $[SiO_4]$ and accordingly formed Al–O octahedral. It is obvious that the alumina particles embedded in the oxide layer come form the Al–O octahedral impurity. It is possible that the local pressure and shearing between the sliding surfaces initiate the bond breakage of Al–O octahedral, and alumina particles were accordingly released.

As a ceramic phase, the hardness of the alumina particles is much higher than that of carbon steels and their oxides. It is easy for them to be embedded in the contact surfaces, and accordingly form a ceramic particle reinforced phase. Moreover, a large number of micron apertures were formed in the case of alumina particles embedded in the contacts. The benefit arising from these apertures on worn surface is a combination of several effects improving oil supply and reducing abrasion in the sliding contact [39,40]. (1) Apertures can act as oil reservoirs, which transport or retain oil to be released in emergency situations. (2) Apertures in friction surface can disarm wear particles by entrapping them, thereby suppressing abrasion and plowing friction. (3) When surface irregularities appear at sufficient density, they can improve the wetting of the surface by oil, and thereby support the lubricating oil film formation.

Physically, occurring dehydration reaction at certain temperature and pressure is one of the most important properties of silicate minerals. So, it is possible for serpentine particles in oil to partly dehydrate due to the local overheating, high flash temperature and high contact stress during the sliding of contact surfaces [41]. Once dehydration reaction occurred, the size of serpentine particles was refined and its hardness was reduced [42]. The particle size would be further decreased by the grinding that initiated by the contact sliding surfaces. That may be the reason why a large number of nano-scale serpentine particles, which acted as the third bodies in friction, were observed on the worn surface lubricated with oil containing surface-coated serpentine UFPs. Traditionally, inorganic silicates such as talcum ($Mg_6Si_4O_{10}(OH)_2$) are among solid lubricants [43]. This is attributable to the four-member-ring stacked layers in certain silicates that are formed from the structural skeleton of silicon and oxygen, $[Si_4O_{10}]_n$. Therefore, the friction and wear could be further reduced due to the uniformly distributed third bodies that formed by refined serpentine particles with a nano-scale diameter.

5. Conclusion

(1) Surface-coated serpentine UFPs suspended in oil present excellent anti-wear and friction-reducing properties. The addition of 1.5 wt% serpentine into oil is found most efficient in reducing friction and wear.

(2) A tribofilm of multi-apertured oxide layer, on which the micrometric alumina particles embedded and serpentine nano-particles adsorbed, is found on surface under the lubrication of oil with serpentine UFPs. It possesses excellent mechanical properties and contributes to the excellent tribological behaviors of serpentine UFPs additive.

Acknowledgments

This research was supported by the Key Basic Research and Development Program of China (2007CB607601) and National Natural Science Foundation of China (50735006, 50805146).

References

[1] Xue QJ, Liu WM, Zhang ZJ. Friction and wear properties of a surface-modified TiO_2 nanoparticle as an additive in liquid paraffin. Wear 1997;213:29–32.
[2] Hu ZS, Dong JX, Chen GX. Study on antiwear and reducing friction additive of nanometer ferric oxide. Tribol Int 1998;31:355–60.
[3] Zhou JF, Yang JJ, Zhang ZJ, Liu WM, Xue QJ. Study on the structure and tribological properties of surface-modified Cu nanoparticles. Mater Res Bull 1999;34:1361–7.
[4] Bakunin VN, Suslov AY, Kuzmina GN, Parenago OP. Recent achievements in the synthesis and application of inorganic nanoparticles as lubricant components. Lubr Sci 2005;17(2):127–45.
[5] Ye PP, Jiang XX, Li S, Li SZ. Preparation of $NiMoO_2S_2$ nanoparticle and investigation of its tribological behavior as additive in lubricating oils. Wear 2002;253:572–5.
[6] Radice S, Mischler S. Effect of electrochemical and mechanical parameters on the lubrication behaviour of Al_2O_3 nanoparticles in aqueous suspensions. Wear 2006;261:1032–41.
[7] Hu KH, Liu M, Wang QJ, Xu YF, Schraube S, Hu XG. Tribological properties of molybdenum disulfide nanosheets by monolayer restacking process as additive in liquid paraffin. Tribol Int 2009;42:33–9.
[8] Tarasov S, Kolubaev A, Belyaev S, Lerner M, Tepper F. Study of friction reduction by nanocopper additives to motor oil. Wear 2002;252:63–9.
[9] Sun L, Zhang ZJ, Wu ZS, Dang HX. Synthesis and characterization of DDP coated Ag nanoparticles. Mater Sci Eng A 2004;379:378–83.
[10] Qiu SQ, Zhou ZR, Dong JX, Chen GX. Preparation of Ni nanoparticles and evaluation of their tribological performance as potential additives in oils. J Tribol 2001;123:441–3.
[11] Zhao YB, Zhang ZJ, Dang HX. A simple way to prepare bismuth nanoparticles. Mater Lett 2004;58:790–3.
[12] Kolodziejczyk L, Martínez-Martínez D, Rojas TC, Fernández A, Sánchez-López JC. Surface-modified Pd nanoparticles as a superior additive for lubrication. J Nanoparticle Res 2007;9:639–45.
[13] Ma JQ, Mo YF, Bai MW. Effect of Ag nanoparticles additive on the tribological behavior of multialkylated cyclopentanes (MACs). Wear 2009;266:627–31.
[14] Peng YT, Hu YZ, Wang H. Tribological behaviors of surfactant-functionalized carbon nanotubes as lubricant additive in water. Tribol Lett 2007;25:247–53.
[15] Pei XW, Hu LT, Liu WM, Hao JC. Synthesis of water-soluble carbon nanotubes via surface initiated redox polymerization and their tribological properties as water-based lubricant additive. Eur Polym J 2008;44:2458–64.
[16] Joly-Pottuz L, Matsumoto N, Kinoshita H, Vacher B, Belin M, Montagnac G, et al. Diamond-derived carbon onions as lubricant additives. Tribol Int 2008;41:69–78.
[17] Lee JK, Cho SW, Hwang YJ, Cho HJ, Lee CG, Choi YM, et al. Application of fullerene-added nano-oil for lubrication enhancement in friction surfaces. Tribol Int 2009;42:440–7.
[18] Hernandez Battez A, Fernandez Rico JE, Navas Arias A, Viesca Rodriguez JL, Chou Rodriguez R, Diaz Fernandez JM. The tribological behaviour of ZnO nanoparticles as an additive to PAO6. Wear 2006;261:256–63.
[19] Wu YY, Tsui WC, Liu TC. Experimental analysis of tribological properties of lubricating oils with nanoparticle additives. Wear 2007;262:819–25.
[20] Hernández Battez A, González R, Viesca JL, Fernández JE, Díaz Fernández JM, Machado A, et al. CuO, ZrO_2 and ZnO nanoparticles as antiwear additive in oil lubricants. Wear 2008;265:422–8.
[21] Chen S, Liu WM, Yu LG. Preparation of DDP-coated PbS nanoparticles and investigation of the antiwear ability of the prepared nanoparticles as additive in liquid paraffin. Wear 1998;218:153–8.
[22] Rapoport L, Leshchinsky V, Lvovsky M, Nepomnyashchy O, Volovik YU, Tenne R. Friction and wear of powdered composites impregnated with WS_2 inorganic fullerene-like nanoparticles. Wear 2002;252:518–27.
[23] Moshkovith A, Perfiliev V, Verdyan A, Lapsker I, Popovitz-Biro R, Tenne R, et al. Sedimentation of IF-WS_2 aggregates and a reproducibility of the tribological data. Tribol Int 2007;40:117–24.
[24] Dong JX, Hu ZS. A study of the anti-wear and friction-reducing properties of the lubricant additive, nanometer zinc borate. Tribol Int 1998;31:219–23.
[25] Zhou JF, Wu ZS, Zhang ZJ, Liu WM, Dang HX. Study on an antiwear and extreme pressure additive of surface coated LaF_3 nanoparticles in liquid paraffin. Wear 2001;249:333–7.

[26] Wang LB, Zhang M, Wang XB, Liu WM. The preparation of CeF_3 nanocluster capped with oleic acid by extraction method and application to lithium grease. Mater Res Bull 2008;43:2220–7.
[27] Yao YL, Wang XM, Guo JJ, Yang XW, Xu BS. Tribological property of onion-like fullerenes as lubricant additive. Mater Lett 2008;62:2524–7.
[28] Ferńandez Rico E, Minondo I, García Cuervo D. The effectiveness of PTFE nanoparticle powder as an EP additive to mineral base oils. Wear 2007;262:1399–406.
[29] Kimura Y, Wakabayashi T, Okada K, Wada T, Nishikawa H. Boron nitride as a lubricant additive. Wear 1999;232:199–206.
[30] Pawlak Z, Kaldonski T, Pai R, Bayraktar E, Oloyede A. A comparative study on the tribological behaviour of hexagonal boron nitride (h-BN) as lubricating micro-particles—an additive in porous sliding bearings for a car clutch. Wear 2009;267:1198–202.
[31] Alexandrov SN. Method of treatment of friction surfaces of friction units. World Patents, WO01/38466, 2001-05-31.
[32] Alexandrov SN. Method of treatment of friction surfaces of friction units. Chinese Patents, CN1317041, 2001-10-10.
[33] Jin YS, Li SH, Zhang ZY, Yang H, Wang F. In situ mechanochemical reconditioning of worn ferrous surfaces. Tribol Int 2004;37:561–7.
[34] Yu Y, Gu JL, Kang FY, Kong XQ, Mo W. Surface restoration induced by lubricant additive of natural minerals. Appl Surf Sci 2007;253:7549–53.
[35] Bec S, Tonck A. Nanometer scale mechanical properties of tribochemical films. Tribol Ser 1996;31:173–84.
[36] Demmou K, Bec S, Loubet JL, Martin JM. Temperature effects on mechanical properties of zinc dithiophosphate tribofilms. Tribol Int 2006;39:1558–1563.
[37] Pereira G, Munoz-Paniagua D, Lachenwitzer A, Kasrai M, Norton PR, Capehart TW, et al. A variable temperature mechanical analysis of ZDDP-derived antiwear films formed on 52100 steel. Wear 2007;262:461–70.
[38] Yu HL, Xu Y, Shi PJ, Xu BS, Wang XL, Liu Q, et al. Characterization and nanomechanical properties of tribofilms using Cu nanoparticles as additives. Surf Coat Technol 2008;203:28–34.
[39] Parry AO, Swain PS, Fox J. Fluid adsorption at a non-planar wall: roughness-induced first-order wetting. J Phys Condens Matter 1996;8:L659–66.
[40] Chow TS. Wetting of rough surfaces. J Phys Condens Matter 1998;10:L445–51.
[41] Tatsumi Y. Migration of fluid phases and genesis of basalt magmas in subduction zones. J Geophys Res 1989;94:4697–707.
[42] Xie HS, Zhou WG, Li YW, Guo J, Xu ZM. The elastic characteristics of serpentinite dehydration at high temperature–high pressure and its significance. Chin J Geophys 2000;43(6):806–11 (in Chinese).
[43] Savan A, Pflüger E, Voumard P, Schröer A, Simmonds M. Modern solid lubrication: recent developments and applications of MoS2. Lubr Sci 2000;12:185–203.